Temperature and density structure of hot and cool loops derived from the analysis of TRACE data

P. Testa, G. Peres, F. Reale

Dip. di Scienze Fisiche ed Astronomiche, Sezione di Astronomia, Piazza del Parlamento 1, 90134 Palermo, Italy – testa@oapa.astropa.unipa.it; peres@oapa.astropa.unipa.it; reale@oapa.astropa.unipa.it

S. Orlando

Osservatorio Astronomico "G.S. Vaiana", Piazza del Parlamento 1, 90134 Palermo, Italy – orlando@oapa.astropa.unipa.it

ABSTRACT

We study the transversal structure (in particular the filamentation) and the longitudinal plasma stratification in two sets of solar coronal loops observed with TRACE in the 171Å and 195Å passbands. The density stratification and the thermal structuring of the plasma along the fibrils which form the loops is derived using simultaneously two techniques: a) filter ratio diagnostic (195Å/171Å) and b) modeling intensity profiles along the fibrils with hydrostatic models; in both techniques we remove the background flux. We find consistent values of temperature and density with both methods in the coronal structures selected.

We find evidence of a very warm fibril ($T \approx 5 \cdot 10^6$ K) and of rather cold ones ($T \approx 2 \cdot 10^5$ K). The hot fibril appears to have a thermal structure with a maximum at the apex compatible with temperature and density stratification, dictated by energy balance, typical of a non-isothermal hydrostatic loop. The cold fibrils appear isothermal and probably in dynamical conditions.

Subject headings: Solar Corona: loops filamentation; hydrostatic models – TRACE

1. INTRODUCTION

Since the earliest spatially resolved observations (Vaiana et al. 1973) it was clear that solar X-ray emitting coronal plasma is confined by the magnetic field in loop-like bright structures, both dynamically and energetically independent. Observations at ever increasing angular resolution have shown the presence of plasma structuring at every spatial scale so far resolved. For example, the rocket-borne Normal Incidence X-ray Telescope (NIXT, Golub 1990), observing for the first time the solar corona in XUV with a resolution of about one arcsecond, showed a fine structuring of coronal loops in many fibrils. Gomez, Martens & Golub (1993), through the Fourier analysis of NIXT images, showed that magnetic structures of all sizes are present, at least down to the resolution limit of the instrument ($\sim$ 0.75 arcsec). The satellite Transition Region And Coronal Explorer (TRACE, Handy et al. 1999), thanks to its arcsecond spatial resolution and large data base of images taken in a few XUV and UV bands, allows us to observe these thin structures systematically since its launch in April 1998.

Previous analysis of coronal loops present in TRACE data (e.g. Lenz et al. 1999; Aschwanden et al. 2000) mainly addressed the structure and the properties of whole bundles of fibrils treated as single coronal loops. Instead, this work focuses on the internal structure of coronal loops and in particular on the properties of single fibrils, i.e. we aim at resolving the internal structure of coronal loops.

The study of the fine structure of coronal plasma has considerable implications because of its connection to the characteristics of physical phenomena that rule the magnetic structuring of the plasma and the spatial distribution of the heating in the solar corona. The presence of thin plasma structures indicates that these driving mechanisms act on very small spatial scales across the loops, and their effects have to be highly localized and structured. Thus studying the transversal structure and the longitudinal stratification of loops has the scope of putting constraint on the fundamental heating and structuring mechanisms. In this respect TRACE allows us to observe coronal structures down to spatial scales smaller than 1000 km. Moreover, since it images the solar corona in three different spectral bands (171Å, 195Å, 284Å), in principle, we can do plasma diagnostics through the filter ratio technique.

The narrow spectral bands of TRACE require special care in the application of the filter ratio diagnostic method, with respect to previous wider band telescopes (e.g. the Soft X-ray Telescope [SXT] on Yohkoh; Tsuneta et al. 1991). This has stimulated us to follow a non-standard multi-way approach to analyze the TRACE data and to investigate morphological and physical conditions of the thinnest element of coronal structures that TRACE can resolve. The application of different analysis methods provide us with cross-checks and allows us to build a robust and consistent scenario. Our analysis method includes the analysis of the observed intensity profiles along the loops and the comparison with standard loop models, which complement filter ratio diagnostics - which we nonetheless use - and provide a check of its results. We will show that this approach not only leads us to obtain a self-consistent scenario, but also to derive fibril characteristics very different from those which would be obtained with the standard TRACE analysis system. In this framework we show that loop fibrils observed with TRACE exist which can be interpreted in terms of conventional loop models, contrary to recent evidence that loops observed by TRACE are non-standard (Lenz et al. 1999; Aschwanden et al. 2000).

In section 2 we show the TRACE data selected and in section 3 we describe the analysis method developed. The results for the two coronal structures analyzed are discussed in section 4. Finally, in section 5 we draw the conclusions of our work.

2. TRACE DATA

Loop filaments are very thin structures with thickness of the order of the resolution element of TRACE. The study of their properties is not trivial, because they can be easily mixed with other adjacent structures, even in the same loop system. In order to simplify the analysis and to isolate the emission of the structure of interest from that of coaligned ones, we looked for structures in a region as free as possible from other bright structures. Usually at the limb the background emission is high because the detector integrates over a longer optical path along the line of sight and thus collects the emission of several structures coaligned with the one of interest. Therefore we have chosen structures on the disk and, in particular, where the background had a simple structure and could be derived in a univocal way.

We selected two observing sequences of the same active region (NOAA Active Region 8297) made with TRACE in August 1998. In the first sequence the active region was, approximately, on the central meridian (1998 August 13); in the second one it was close to (but not on) the west limb of the Sun (1998 August 19). Fig. 1 shows some of the TRACE images and the location of their field of view in full-disk Yohkoh/SXT X-ray images.

Each observing sequence contained couples of images taken in different filter bands (171Å and 195Å). In the images of August 13 (upper panels in Fig. 1) several fibrils composed a loop and it was possible to analyze the plasma structure along and across the loop; at least one fibril was entirely visible from a footpoint to the other. In August 19, the active region was close to the limb and the analysis required more attention due to the more extended superposition of several coronal structures along the line of sight. We analyzed, in particular, a system of fibrils evident in the lower part of the TRACE field of view (see lower panels of Fig. 1). Only the lower parts of the fibrils were visible; on the other hand there was only limited contamination from nearby bright structures.

The TRACE observing sequence on 19 August covered several hours with a time resolution of, approximately, 1 minute for each band, so we also had the opportunity of looking

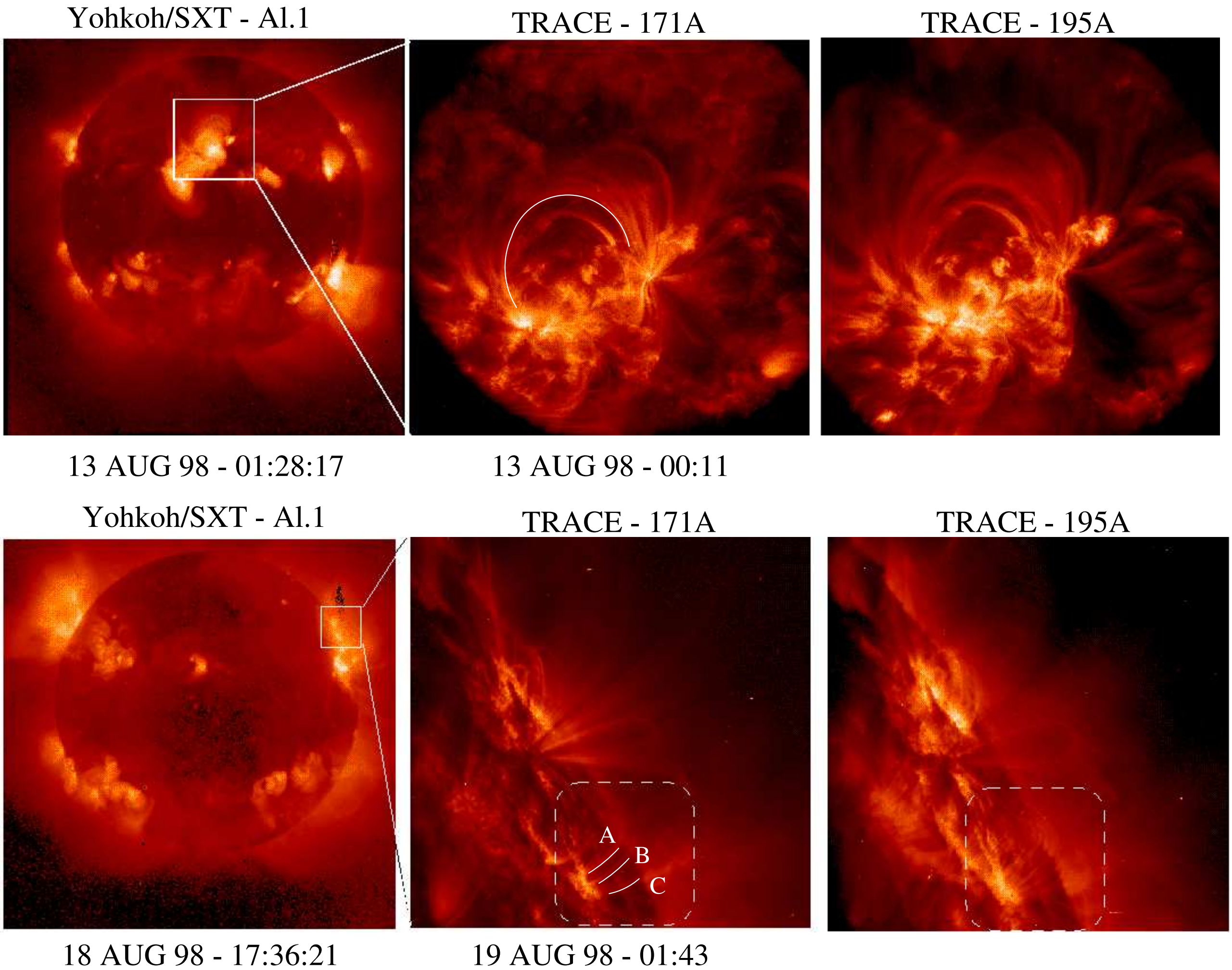

Fig. 1.— Images of the coronal structures analyzed, all belonging to the same AR but observed six days apart. Upper panels – left: full disk image collected with Yohkoh/SXT through the filter Al.1 on August 13, 1998, together with the field of view (FOV) of TRACE; center and right: TRACE images in the two bands, 171Å and 195Å, showing the loops system analyzed; the white line marks the fibril analyzed in detail. Lower panels – As in the upper panels, for the data collected six days later; the dashed box contains the fibrils analyzed, marked with the white lines.

at the evolution of these fibrils. We have studied the evolution of the fibrils for ~ 1 hour but the relevant results are not shown in this paper.

3. METHOD OF ANALYSIS

Since we aim at studying in detail the fine structure of coronal loops using TRACE data at 171Å and 195Å, we have analyzed the structure across the magnetic field, and the temperature and density stratification along the loop, i.e. along the magnetic field lines.

We analyze the plasma physical properties with two techniques based on different physical principles both leading to temperature, T, and emission measure, EM, (or density) derivation. In particular, the technique to derive the physical properties across the loop is different from that used along the loop. We derive T and EM profiles *across* the loop through filter ratio diagnostic (I_{195}/I_{171}) in each pixel after proper background removal; instead, to derive the structure *along* the loop we fit the observed intensity profiles in each band with intensity profiles synthesized from temperature and density vs. field line coordinate, s, of hydrostatic loop models.

A more detailed analysis of the filter ratio usage is given in appendix A. When using the filter ratio technique, we consider the range of temperature over which the filter response is larger than 0.1% of the peak, namely 10^5 K $\lesssim T \lesssim 10^7$ K. This temperature range is much larger than the narrow range of temperature commonly used in the *standard analysis*, $0.9 \div 1.8 \cdot 10^6$ K. In case of a filter ratio yielding more than one temperature value, we select the temperature consistent with the fitting with hydrostatic models.

The value of the filter ratio may be significantly altered if the flux includes signal from other structures coaligned along the line of sight. Therefore, before computing filter ratio, it is important to estimate accurately and remove such a background emission. The background cannot be subtracted automatically because it is not pure noise, but consists also of the emission from coherent structures (other fibrils or plasma blobs) coaligned with the ones selected for the analysis and its subtraction will be described in detail below. This problem has been preliminarily reduced by having selected carefully fibrils that stand out and are as isolated as possible.

3.1. Loop transversal structure

We studied the intensity profiles *across* loops and sampled the transversal structure at several places along the loop. The sampling was regular with care to avoid points of intersection with other bright structure along the line of sight. Fig. 2 shows how each *transversal* profile has been obtained (s_T is the coordinate across the loop). To increase the signal to noise ratio and thus to single out the loop fibrils better, we sum the signal over small strips, each 1 pixel wide and 8 pixels long, aligned with the fibrils. Fig. 2 includes an example of *transversal* intensity profile. The background emission at each place along the loop is obtained as a rectilinear, lower envelope of the profile: we assumed that profile minima yielded the background emission, and we interpolated between them.

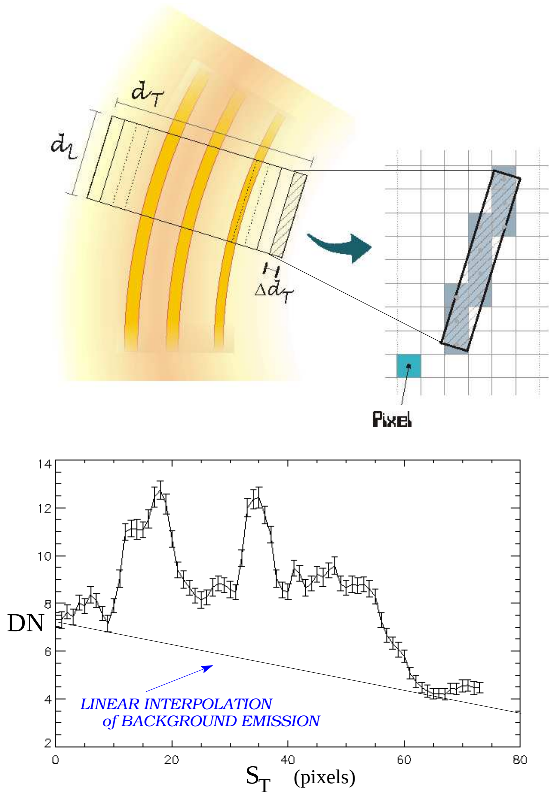

Fig. 2.— Top – Sketch of a section of a loop made of many fibrils (arch-like structures) with an example of a band of strips used to measure the brightness *across* the loop. Each strip is 1 pixel wide and 8 pixels long, aligned to the fibrils; the enlargement on the right shows an example of the 1×8 pixels strip and the pixels included. We integrate the brightness along each strip to obtain a single value little affected by statistical fluctuations. Bottom – An example of a real intensity profile measured *across* a loop with this method (s_T is the coordinate across the loop). The evident peaks in the profile help us to identify the various fibrils. The solid straight line is our interpolated background profile, to be subtracted from the measured profile.

To define operatively the fibrils width on the basis of the *transversal* intensity profiles, we fitted the profiles of the evident fibrils with gaussians, and took the width of each gaussian as the characteristic thickness of the fibril. From the ratio of background-subtracted intensity profiles in two spectral bands (171Å and 195Å), we derived *transversal* profiles of temperature and emission measure. As discussed above, we did not restrict ourselves to the range around

10^6 K, as instead it is usually done in the TRACE *standard analysis*, but we considered a wider temperature range.

3.2. Density and temperature stratification along loop fibrils

Intensity profiles *along* the fibrils has been measured over a path as close as possible to the fibril centre. To derive the plasma physical conditions we assumed each fibril to be in equilibrium and described it with hydrostatic loop models. Then we derived the plasma temperature and pressure from a fit, simultaneous in the two bands, of these *longitudinal* intensity profiles with hydrostatic loop models. We first considered, as a simple first assumption, an isothermal hydrostatic model; in case of unsatisfactory agreement with observed profiles we considered a more complex non-isothermal (Serio et al., 1981; hereafter S81) hydrostatic model that takes into account the detailed energy balance and hydrostatic equilibrium of the plasma inside the loop. Uncertainties on *data numbers* (DN, proportional to the brightness detected) are derived assuming a Poisson distribution of the corresponding detected photons.

For the analysis of the *longitudinal* structure, we derived the background emission from that obtained in the analysis of the transversal structure: from each transversal background profile we took the value at the fibril position, obtaining several background values almost regularly spaced along the fibril; we then interpolated among them to have a complete background longitudinal profile.

Since some works (Aschwanden et al. 2000; Lenz et al. 1999; Reale & Peres 2000; Brekke et al. 1997; Foukal 1976) have discussed cases of isothermal plasma in a loop, we consider this possibility in our modeling effort; the surface brightness profile expected in this case in each passband is an exponential decreasing from the footpoints to the apex. In order to fit one loop's leg, we have therefore used the functional form for such a brightness profile as:

$$I_f(s) = A_f \cdot e^{-(s-s_0)/L} \tag{1}$$

where L is the brightness scale-height (which is the same as the emission measure scale-height for an isothermal plasma) and being one half of the pressure scale-height, which depends just on temperature, allows us to find the temperature; s_0 is the reference point where we calibrate A_f, that is the normalization factor defined as:

$$A_f = R_f(T(s_0)) \cdot n^2(s_0) \cdot t_{exp} \cdot C_d$$

where t_{exp} is the exposure time, C_d is the column depth, and $R_f(T)$ is the filter response to an isothermal plasma (shown in Fig. 12 of appendix A) vs. plasma temperature T. $R_f(T)$ is the coronal plasma emission obtained with the CHIANTI (Dere et al., 1997) spectral synthesis model and folded with the instrument spectral response. Then, assuming the temperature of the isothermal model and the column depth equal to the width obtained from the analysis of the transversal structure, we derive a density value. The above functional form (eq. 1) suffices to tackle the study of incomplete loop such as the ones observed on August 19; for a complete loop such as the one observed on August 13, one can use an exponential for each leg, namely the one of Eq. 1 for one leg, and $A_f \cdot e^{(s-s_0)/L}$ for the other leg, with the same meaning of the symbols. It is worth noting that s_0, in this case, is the pixel where one matches the profiles of the two legs and which is located at the loop apex; L, depending just on temperature in the loop, has to be the same on both legs; in order to have symmetry the two exponentials have to match at the loop center (apex). For this model the fitting parameters are: the scale-length of the exponential (i.e. essentially the isothermal temperature), the values of normalisation constants in the two bands and the position of the apex.

The S81 hydrostatic loop model considers energy balance among the radiative losses, the divergence of heat flux and an heating term here assumed uniform (but easily modifiable to account for any heat distribution); it also considers hydrostatic pressure balance under the effect of gravity and the equations system is solved self-consistently, yielding profiles of temperature and pressure along the loop. In the case of the hydrostatic non-isothermal S81 model, the data have been compared to surface brightness profiles derived from the density and temperature computed with the model. We generated a grid of 100 models with different maximum temperature in the range 10^5 K $\div 10^7$ K, equally spaced in maximum temperature T_{max} with constant $\Delta log T_{max} = 0.02$; the base pressure is tied to the temperature by the scaling laws; the loop length is derived from the images and the heating is assumed uniform. From the profiles of density and temperature along the loop, the relevant intensity profiles are synthesized as:

$$I_f(s) = \alpha_f \cdot n^2(s) \cdot R_f(T(s))$$

where α_f is a normalisation constant proportional to the emitting plasma volume. The parameters of the fit, in this case, are the two normalization constants, one per band, the location of the symmetry center of the model with respect to the observed profiles, and T_{max}, the loop maximum temperature.

For both models, i.e. the isothermal and the not-isothermal one, we include the effect of loop inclination (we consider the component of gravity along the field line coordinate in the hydrostatic models) as deduced through morphological analysis of TRACE images. Since the complete loop seen on August 13 appears semicircular in the images, the most likely morphology is that it is indeed semicircular and lies in a plane perpendicular to the line of sight; any other geometry, e.g. a rather elongated ellipsoidal loop appearing semicircular for projection effects, is rather artificious and highly unlikely; it would also imply a significant stretching of the magnetic field. Then the inclination with respect to the solar surface is approximately equal to the latitude of the loop system in solar coordinates, i.e. about 30°. Instead, for the fibrils observed on August 19, we assumed that they are perpendicular to the surface as they appear in the images.

We required that each model fitted all the observations, i.e. simultaneously both the brightness profiles got at 171Å and at 195Å. This, furthermore, automatically grants to get the right filter ratio along the fibril. The fitting consisted in looking for the lowest χ^2 value in the parameter space of the model under scrutiny; note that the parameters are different for the isothermal loop model and for the non-isothermal (S81) one. The uncertainties on best-fit parameters are derived from the 68% confidence levels drawn in the parameter space around the best fitting values as in Avni (1976).

4. RESULTS

The two groups of fibrils observed, in the same active region but at different times, revealed very different physical properties. We now describe in detail the results found for each of them.

4.1. August 13 data

In the August 13 observation, a system of extended coronal loops is well visible (Fig. 1). Their apparent length is about 10^{10} cm. The right leg of the loop system is highly structured with many, clearly evident, fibrils. The fibrils get ever less defined from the right footpoint to the apex and from there toward the other footpoint, to which irregular brighter structures are superimposed. Nevertheless there is a central fibril entirely visible and well defined, mostly in the 171Å band.

To study in detail the filamentation of this loop system, we sampled the trasversal profile at several points along the loop as shown in Fig. 3.
Fig. 4 shows an example of transversal profiles in the two bands. We found that both the thickness of the fibrils and the distance between them appear to increase from the footpoint to the apex. For example, the width of the central fibril increases from $3.6\ (\pm 0.4) \cdot 10^8$ cm ($\sim$ 5 pixels) near the right footpoint, to $8.4\ (\pm 0.8) \cdot 10^8$ cm ($\sim$ 12 pixels) near the apex. Moreover different fibrils can have very different widths in a wide range: $1.8 \cdot 10^8 \div 10^9$ cm, as clear in Fig.4.

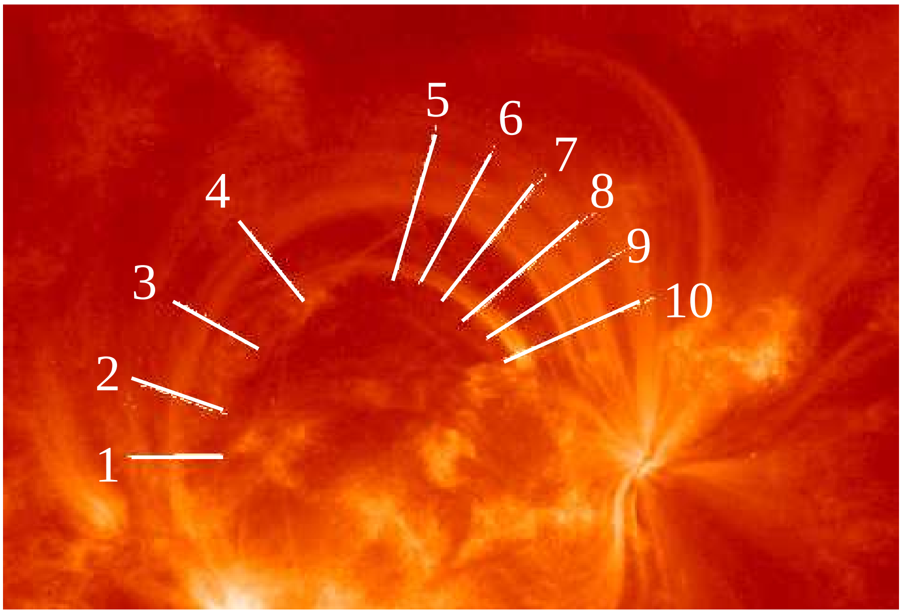

Fig. 3.— The active region near the central meridian, as observed on August 13, through the 171Å filter of TRACE; the paths where we sampled the transversal intensity profiles are marked on the image as white, numbered lines.

From the analysis of the transversal structure we found, inside the fibrils, values of 195Å/171Å fluxes ratios approximately in the range $1 \div 2$, i.e. compatible with plasma tem-

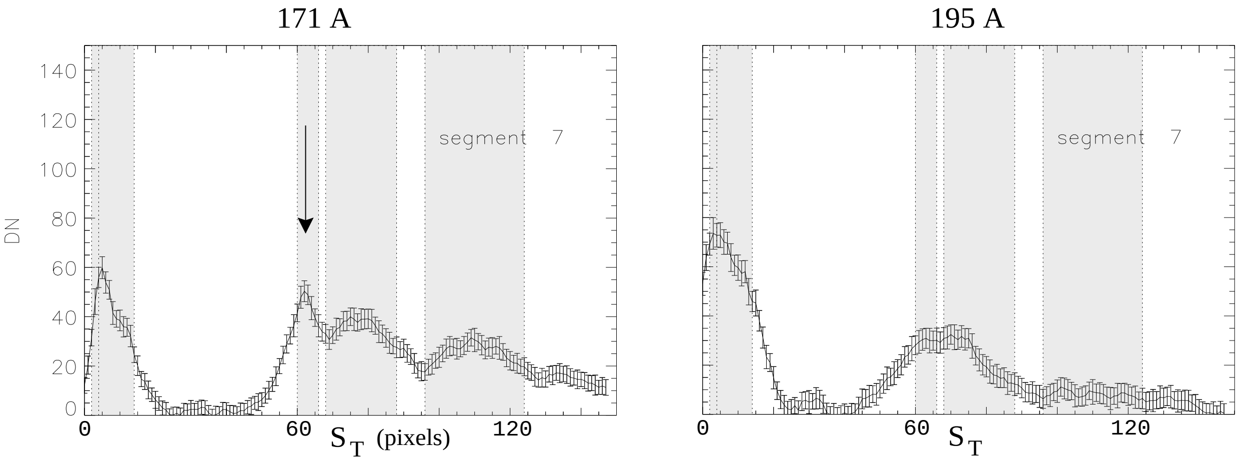

Fig. 4.— Intensity profiles (DN/pixel) along the segment 7 of Fig. 3 after background removal. $s_T = 0$ corresponds to the concave (inner) part of the loop. The grey regions show the width of the fibrils, as defined by the fit to the profile with gaussian functions in the 171Å band; the arrow points at the fibril entirely visible, from one footpoint to the other.

perature of about $1.5 \cdot 10^6$ K or, alternatively, since the temperature vs ratio is multivalued, of a few million degrees (see Fig. 12 in appendix A). As discussed below, the analysis of the emission properties along the loop allowed us to remove such an indetermination and to discriminate between the different temperature ranges.

As for the longitudinal structure of the fibrils, we show now the results obtained for the fibril, mentioned above, entirely visible (marked with a white line in the upper central panel of Fig. 1). Due to its complete visibility, this fibril allowed us to discriminate between the two hydrostatic models.

This fibril is quite long (its half length is about 250 pixels, corresponding to $\approx 9 \cdot 10^9$ cm), and provided us with many data points for the analysis of the structure *along* the loop; to increase the signal to noise ratio we binned the longitudinal emission profiles over 4 pixels, along the white line (see Fig. 1), and we obtained, excluding the region close to the footpoints, about 100 data points for each band.

Table 1: Best-fit parameters of non-isothermal model

Length of the loop	$8.8 \cdot 10^9$ cm
Temperature at loop apex	$5.2 \pm 0.3 \cdot 10^6$ K
Pressure at the base	5.2 ± 0.8 dyn cm^{-2}
Density at loop apex	$3.2 \pm 0.3 \cdot 10^9$ cm^{-3}
Column depth in 171Å band	$3.8 \pm 0.5 \cdot 10^9$ cm
Column depth in 195Å band	$2.5 \pm 0.4 \cdot 10^9$ cm
χ^2_r	1.1
degrees of freedom	196[a]

[a] Two data sets of 100 data points are fitted simultaneously

A first fitting of the observed profiles with the isothermal plasma model, yielded a best-fit temperature $T = 2.2 \cdot 10^6$ K [1] but a reduced chi-squared $\chi^2_r = 2.1$. Assuming circular cross-section of diameter 5.4 $(\pm 0.6) \cdot 10^8$ cm (derived from the analysis of transversal profiles), we obtained for the density at the apex a value of $2.5 \cdot 10^9$ cm^{-3} from the 171Å normalisation constant, and $2.0 \cdot 10^9$ cm^{-3} from that of the 195Å band, i.e. two values not in disagreement.

We found however a much better agreement of the data with the S81 model. The physical properties of the best-fit S81 model (in particular, L/2, T_{max}, p_{base}, n_{apex}, column

[1] Note that this temperature, found by forcing isothermal conditions, is nonetheless outside the range allowed by *standard analysis*.

depth in 171Å and 195Å bands) are summarized in Table 1.

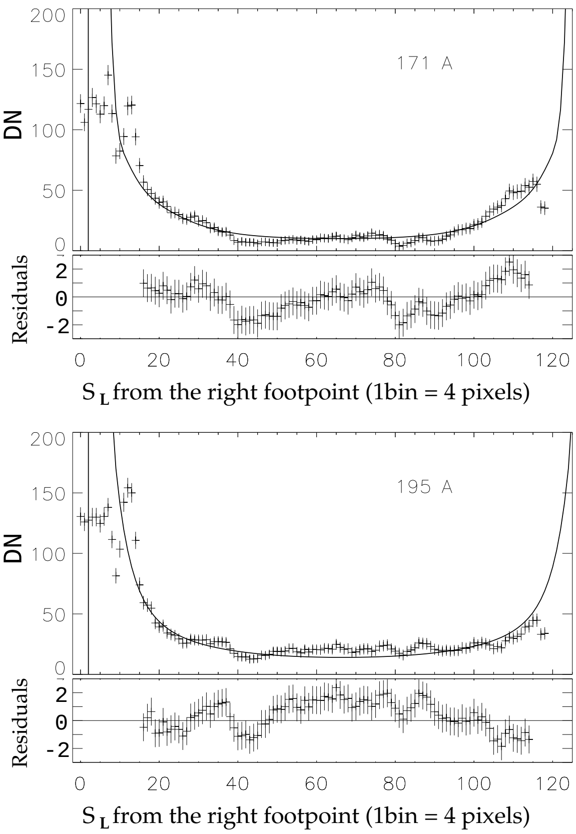

Fig. 5.— *Longitudinal* intensity profiles at 171Å (upper panel) and 195Å (lower panel) for the semicircular fibril (marked in Fig. 1) observed on August 13, 1998. The data points are the rebinned measured values (a bin corresponds to 4 pixels) and the solid lines are the intensity profiles synthesized from the temperature and density profiles computed with the most recent version of the S81 hydrostatic loop model, and best fitting the brightness profiles simultaneously in both bands. The best fit model is a loop with the apex at $T \simeq 5.2 \cdot 10^6$ K and pressure at base about 5 dyne cm^{-2}. Below each graph we show the related fit residuals.

The values of the integration depth over which the emitting plasma extends along the line of sight are derived from the normalization constants of the model profiles (the normalisation constant is, in fact, the product of integration depth and exposure time). The integration depths are of the order of $3 \cdot 10^9$ cm. Fig. 5 shows the data and the best fit model: the agreement is clearly good (and, in fact, $\chi^2_r \approx 1.1$). Fig. 6 shows the related χ^2_r plane of the fitting, with the confidence levels at 95% and 99%, as a function of maximum temperature

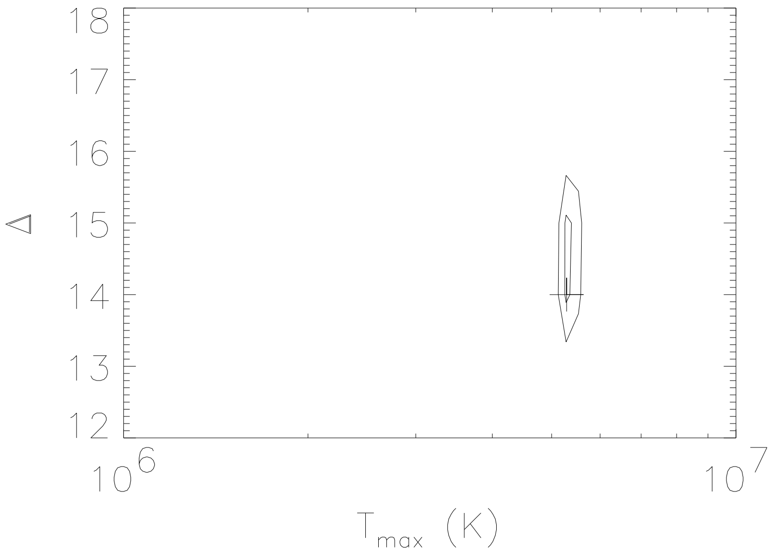

Fig. 6.— Plane of the fitting parameters with the S81 model: χ^2 contours vs. the displacement Δ of the loop model apex from the middle point of observed profiles (in units of bins of 4 pixels, as for s_L in Fig. 5), and vs. the maximum temperature T_{max} of the S81 model. The position of minimum χ^2 is marked with a cross. Contours at confidence levels 95% and 99% are shown.

of the model and of the position of the loop apex with respect to the center of the data coordinates. A second local χ^2 minimum has been found at a different temperature, namely $7 \cdot 10^5$ K; we can exclude it because of its much higher χ^2 value ($\chi^2_r \sim 2$) and of physical considerations. In fact, for this model the normalization constants are very different in the two bands by about one order of magnitude and lead to integration depths ranging between 10^{12} cm and 10^{13} cm which, of course, do not make sense; moreover the temperature found is not compatible with the fluxes ratios observed. Instead, the best-fit temperature of $\sim 5 \cdot 10^6$ K is compatible with the filter ratio found at various points sampled with the analysis of transversal structure.

In the light of the above discussion, we can conclude that this almost semicircular fibril, entirely visible, can be adequately described as a rather hot ($T_{max} \simeq 5.2 \cdot 10^6$ K) non-isothermal coronal loop with a "normal" energy balance according to the S81 model and uniformly heated.

4.2. August 19 data

In the TRACE images at limb, taken on August 19, the whole active region has a more complex aspect, with several bright and irregular structures. The fibrils selected come out from a very bright base and appear very similar to each other as for both luminosity and morphology. In the 171Å image, they are bright and with sharp edges, while the regions in between are dark. Instead, in 195Å image the "inter-fibril" regions are generally slightly brighter. These fibrils were observed over several hours and their brightness showed some slow variability, while, neither their geometry nor their length appeared to vary. Fig. 7 shows the region of the fibrils and four paths along which we studied the transversal structure of the fibrils.

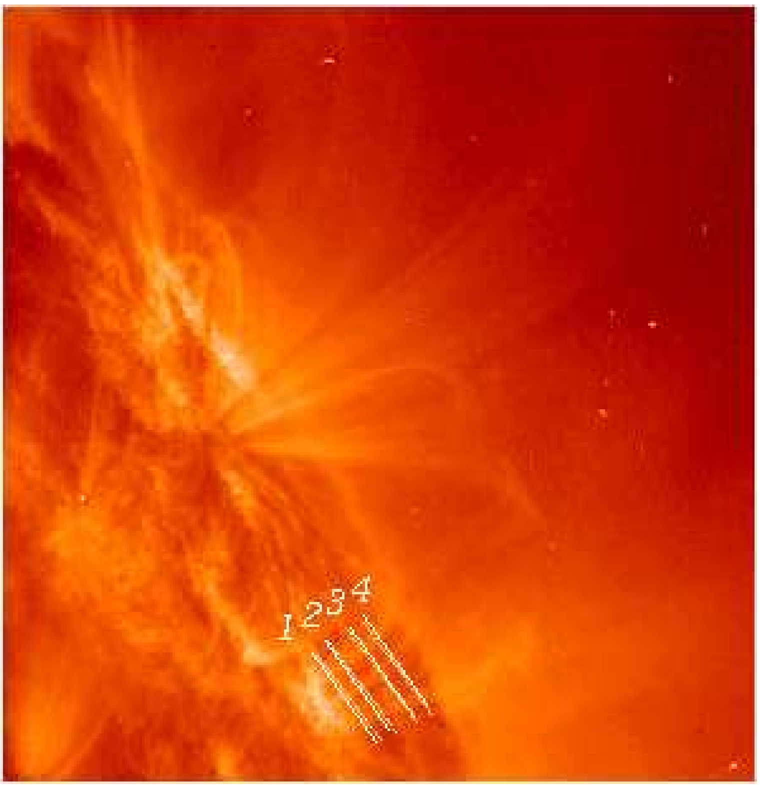

Fig. 7.— The active region near the limb, as observed on August 19, through the 171Å filter of TRACE. On the image the white lines mark the paths where we sampled the transversal intensity profiles.

As an example, Fig. 8 shows the transversal profiles obtained along segment 3. We found that these fibrils have similar thickness, almost constant along the fibrils, with values in a range $1.4 \div 4.2 \cdot 10^8$ cm ($2 \div 6$ pixels); note that, the lower values are comparable to the spatial resolution of TRACE.

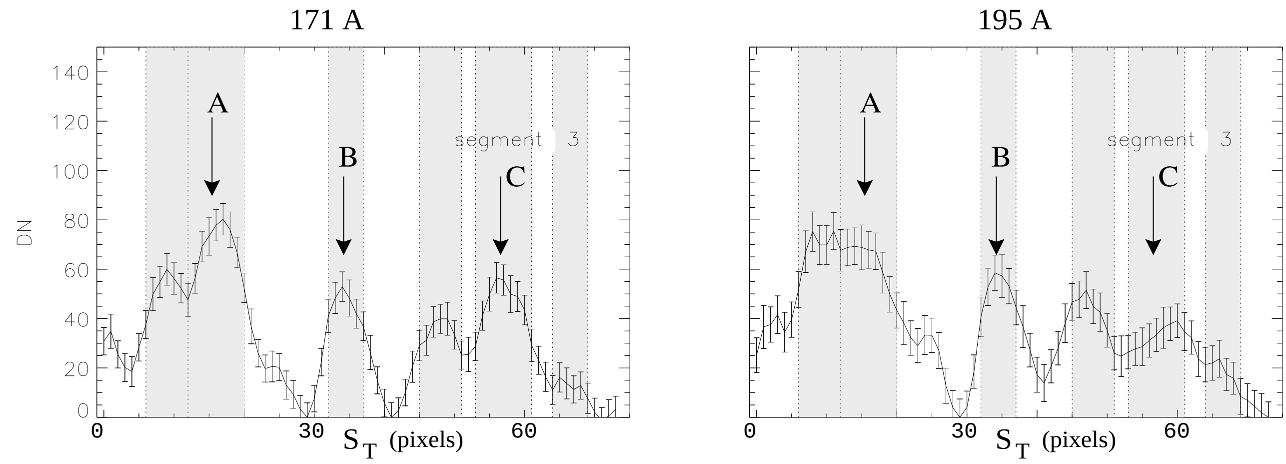

Fig. 8.— Intensity profiles (DN/pixel) along the segment 3 of Fig. 7 after background removal. $s_T = 0$ corresponds to the upper extreme of the segment. The grey regions are the fibrils as defined by the fit to the profile with gaussian functions. As in the previous case, the arrows point at the fibrils, marked with white lines in the lower central panel of Fig. 1.

We now discuss the structure *along* the fibrils. The fitting of each longitudinal profile was not possible with a complete loop model since the fibrils are clearly only part of longer loops and it is virtually impossible to constrain a coronal loop model with information on only a small fraction of the loop. On the other hand, as shown in Fig 9, we found no evidence of thermal stratification along the fibrils. All the profiles along the three fibrils in fact show a

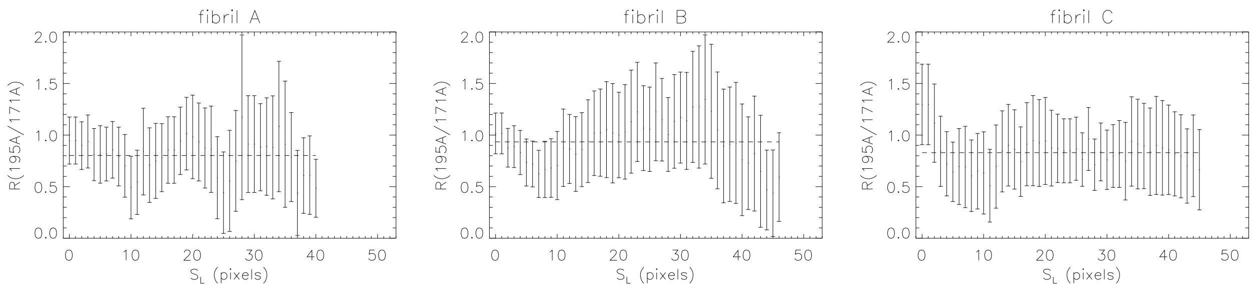

Fig. 9.— Profiles of the ratio of fluxes (195Å/171Å) along the three fibrils marked in Fig. 7. $S_L = 0$ corresponds to the footpoint of each fibril. The dashed line in each plot correspond to the mean value of R(195Å/171Å).

good agreement with the exponential trend of a purely isothermal model. Fig. 10 shows the best-fit model profiles superimposed to the data. In both 171Å and 195Å profiles, and for all the three fibrils considered, the evident bump is due to another bright structure evident in the images and running across the fibrils: in order to avoid contamination it was excluded from the fitting.

Table 2: Best-fit parameters of isothermal model, August 19 loop

fibril	T (10^5 K)	n_{base}[a](10^{10} cm^{-3})		χ^2_r	dof
		171Å	195Å		
A	$2.7^{+1.2}_{-0.6}$	$0.7^{+0.5}_{-0.3}$	$0.9^{+0.8}_{-0.1}$	0.24	48
B	$1.8^{+0.2}_{-0.2}$	$3.4^{+0.7}_{-0.8}$	$3.5^{+1.9}_{-1.1}$	0.27	60
C	$2.6^{+1.2}_{-0.7}$	$0.5^{+0.5}_{-0.2}$	$1.0^{+1.0}_{-0.1}$	0.14	65

[a]The density is derived from the normalization factors of the fitting in each band (i.e. the constant A_f of Eq. 1 in section 3.2)

The physical parameters that characterize the best-fit model for these three fibrils are summarized in Table 2. Assuming that the fibrils are perpendicular to the solar surface, we obtained for the best-fit model a scale-height that correspond to a temperature of $2.7 \cdot 10^5$ K for fibril A (see Fig. 1 for the fibrils label), $1.8 \cdot 10^5$ K for fibrils B and $2.6 \cdot 10^5$ K for fibrils C; these temperature values are consistent with the filter ratio values obtained from the transversal structure analysis. Normalisation leads to density values of the order of 10^{10} cm^{-3} with good agreement between the results of the two bands. Notice that the best-fit temperatures of these fibrils are much lower than the temperature of the best-fit loop model in subsection 4.1.

5. DISCUSSION and CONCLUSIONS

In this work we have studied the morphology plus the density and thermal structuring of two groups of coronal structures of the same AR observed six days apart. Our analysis has shown that the fibrils that compose all these structures can be of different width down to the spatial resolution limit: we have singled out and analyzed fibrils of width comparable with 1 arcsec. Thanks to the superior TRACE angular resolution we have been able to study systematically these basic elements of the coronal structures down to the spatial scales presently accessible.

The two regions studied show different characteristics of filamentation. The one observed on August 13 is characterized by fibrils of very different width, in the range $4 \cdot 10^8 - 2 \cdot 10^9$ cm. The width of each fibril appears to vary with height, in some case even by a factor 2; however

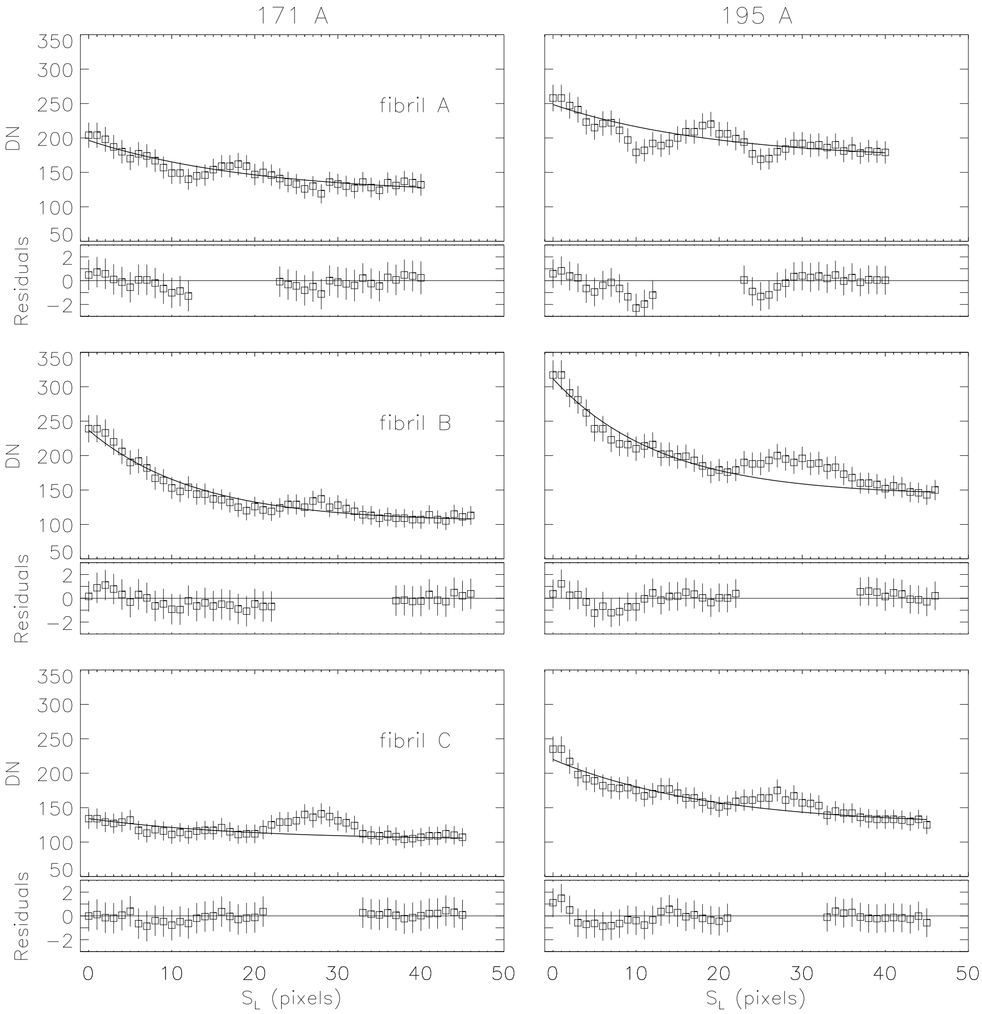

Fig. 10.— Intensity profiles at 171Å (left) and 195Å (right) *along* the three fibrils observed on August 19, 1998 (data points). The solid lines are the intensity profiles synthesized from the temperature and density profile computed with a model of *isothermal* loop in hydrostatic conditions, and best fitting the brightness profiles simultaneously in both bands. The best fitting temperature is about $2.7 \cdot 10^5$ K for fibril A, $1.8 \cdot 10^5$ K for fibrils B and $2.6 \cdot 10^5$ K for fibrils C; the derived density values are of the order of 10^{10} cm^{-3}.

near the apex, the fibrils are less defined and distinguishable, so we may be grouping together more than one fibril. Instead, the selected fibrils of August 19 look more similar to each other and all seem to have a characteristic width of about $3 \cdot 10^8$ cm, close to the spatial resolution limit. For this system, the fibrils width appears to be constant with height as far as it is possible to verify.

A common characteristic of both sets of observations is the presence, in a loop complex, of several truncated fibrils, i.e. fibrils with only one leg visible, whereas standard hydrostatic loop models (Rosner, Tucker & Vaiana 1978; S81; Vesecky et al. 1979) predict symmetric loop legs. Perhaps these fibrils are rather extended loops that become fainter and fainter near the apex, and we are not able to follow them to the other leg; another possibility is that the heating could be distributed highly asymmetrically along the loop; or they could be non-symmetric magnetic configurations or even non-hydrostatic loops: the plasma inside these fibrils could be in different physical conditions at the two footpoints and plasma flows could be present. The analysis of this latter kind of fibrils probably needs to consider hydrodynamic models that involve asymmetry of density and temperature distribution and therefore could explain the observed brightness asymmetry; even more, some of these loops may be subject to slow changes and, if this is the case, a time-dependent hydrodynamic model may be more appropriate to describe their characteristics.

Besides the morphology discussed above, the detailed analysis of the physical characteristics has shown a rather complex scenario. In the case of the region observed on August 13 we could analyze a whole fibril from one footpoint to the other obtaining interesting constraints on the model and on the data analysis. We carefully modeled the observed profiles and exploited the hydrostatic models as diagnostic tools. As discussed in subsection 4.1, we have found for this fibril a fairly good agreement between the observed longitudinal profiles and those derived from S81 hydrostatic loop model at a rather high maximum temperature ($\sim$5 MK); an isothermal model cannot instead reproduce the observed profiles. In any case, with both models we invariably find values of best fit temperature significantly higher than 1 MK. Moreover, the finding that these fibrils are typical coronal loops at a temperature of a few million degrees is consistent with the presence of very hot loops observed by Yohkoh/SXT in the same region and almost simultaneously. In fact, given the plasma parameters derived for this fibril ($n_e \sim 10^9$ cm^{-3} and $T \sim 5$ MK; see Tab. 1), these loops should be visible in images taken with Yohkoh/SXT that has a high sensitivity to hotter plasma. To inspect this point, we carefully coaligned the two images collected in TRACE/171Å and SXT/Al.1 passbands, taking into account also the shift due to the solar rotation (SXT observed the examined region about one hour and half after the TRACE observation). Fig. 11 shows the contours of the TRACE/171Å image (of the upper central panel of Fig. 1) superimposed to the SXT/Al.1 image; when comparing the observations of the two instruments one has to consider that the Yohkoh/SXT angular resolution is five time worse than the resolution of TRACE. *It is worth noting that while some of the structures observed with TRACE match well bright structrures seen with SXT, some other loops, instead, do not match in the two observations. From the comparison of the two observations we can see that the fibril examined in the present work falls at the border of a rather bright region in Yohkoh data, so,*

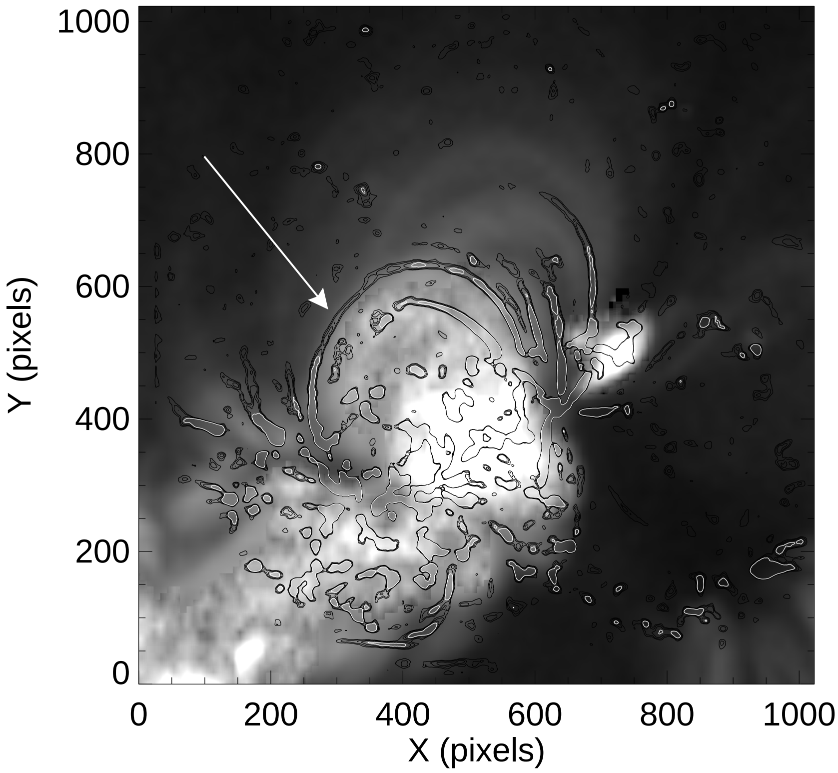

Fig. 11.— Yohkoh data with contours of TRACE/171Å data superimposed. The Yohkoh image is the composition of two Al.1 observations of different exposure time, in fact the long time observation has several saturated pixel in the central very bright region. The spatial unit of length is the size of TRACE pixels. The arrow marks the fibril analyzed in details.

as far this fibril is concerned, it corresponds to structures observed with Yohkoh/SXT. As an additional check we have synthesized the DN numbers at the Yohkoh/SXT focal plane that the relevant best fitting hot loop model should generate, if observed through the Al.1 and AlMg bands, and we found a good agreement with the numerical values in the Yohkoh data. *It is worth noting that the object of this work is neither a complete analysis of all the structures in that region, nor a detailed comparison between the observation of TRACE and Yohkoh/SXT: we just analyzed a single fibril observed with TRACE, and found its structure and emissivity most reasonably explained as being hot. Thus, the results of this analysis do not apply in general to the whole band of fibrils visible with TRACE; what we found is in fact that it is necessary to analyze every single fibril separately.*

An interesting result of our analysis is the large integration depth we have found fitting the data with the loop model (similar results are already in Lenz et al. 1999, and in Priest et al. 2000). Such an effect could depend on several reasons. The structures analyzed may for instance be really "thick" (i.e. being ribbon-shaped or arcades). Another possibility is the presence of systematic effects in the evaluation of emission measure from data, e.g. if the metal abundances were underestimated for any reason. Notice that a loop model with a uniform heating distribution is enough to fit the data satisfactorily; this is for instance in agreement with the results of Priest et al. (2000). Given the goodness of the fit we have not explored other, more complex, spatial distributions of heating. Notice also that the best-fit non-isothermal model predicts the presence of footpoints in TRACE bands brighter than observed. This effect may at first glance lead to reject the model but looking at the data (Fig.5) one may reasonably think that the observed loop footpoints are "truncated". This may be due to the overlap of a lot of other low lying structures, which may make the plasma optically thick and obscure the footpoints, located deeper in the atmosphere. Other possible explanation include a tapering of the loop in the transition region, although this seems to be typical of even lower layers (Vaiana & Rosner 1977); finally another explanation is that the loop thickness is below the TRACE resolution and the integration of the emission in a pixel may dilute prominent emission peaks.

At variance with the results of other recent analysis of TRACE data (Aschwanden et al. 2000; Lenz et al. 1999), our work suggests a variety of loops over a large range of temperature; some are isothermal, others are not compatible with an isothermal plasma. In particular, for the only complete loop fibril we could analyze we have found good agreement of data with standard non-isothermal loop models. Recent works claim, on the other hand, that most loops observed with TRACE are at 10^6 K and cannot be described with classical loop models and appear to belong to a class of loops new with respect to those observed with other X-ray instruments like Yohkoh. The different results we obtained may depend on having compared the loop model with the emission of one fibril accurately singled out, rather than with a wide transversal region including the emission of several fibrils. In fact, it has been shown that summing together the emission of fibrils with different temperature could lead to emission profiles which may be taken as a single isothermal loop (Reale & Peres 2000; Schmelz et al. 2001). Among many recent works that, on the other hand, found evidence of thermal structuring inside loops, we mention Priest et al. (2000) who modeled the emission of a loop observed with Yohkoh/SXT finding good agreement with a hydrostatic non-isothermal uniformly heated loop. Our analysis indicates that TRACE is able to detect also structures at several million degrees, typically detected in Yohkoh observations.

The fibrils selected in the image of August 19 appear significantly different from that of August 13. In fact their morphological properties seem more uniform, as already mentioned, and also the temperature and density values seem more homogeneous: they are all well described by an isothermal model with a density of about 10^{10} cm^{-3} and a low temperature (T $\sim 2 \cdot 10^5$ K) compatible, as in the previous case, with the values of filter ratios obtained by the transversal structure analysis. These characteristics suggest a strong analogy with cold loops observed in UV lines (Foukal 1976; Brekke et al. 1997; see also Peres & Orlando 1996). For these cold loops, because of their temperature, we checked whether they were possibly detected in the simultaneous UV TRACE observations at 1550Å and 1600Å, more sensitive to colder plasma. We examined these simultaneous UV observations and found no evidence of the loops. However, from the temperature and density values of the relevant best fit models (see Tab. 2), we computed the emission of the three analyzed fibrils in these passbands. The synthesized profiles along the three fibrils are rather lower than the observed fluxes, and then their emission is compatible with being swamped by the background noise and other plasma structures brighter in these UV bands.

All things considered, our analysis method led to temperature and density distributions typical of hot coronal loops for the fibrils observed in August 13, near the central meridian, whereas the fibrils observed near the limb on August 19 appear very cold and without any evident thermal structuring. It is interesting to note, therefore, that both cases studied in detail show a scenario quite different from the loops at $T \sim 10^6$ K invariably found with *standard analysis* and probably more complex than discussed by Aschwanden et al. (2000). *It is equally worth noting that we model individual loops, that our approach in this work is to study loops one by one, and, therefore, our results cannot be generalized to all loops observed with TRACE.*

Given their importance for the mechanisms of heating through the dissipation of mechanical and magnetic energy, studies of the coronal fine structure are quite important. In this perspective a careful and detailed analysis of TRACE data is in order in the light of future solar missions, which, in order to investigate the fine structure of the solar corona, are pursuing higher spatial resolution either by means of technological improvements or orbiting closer to the sun (e.g. Solar Orbiter; Colangelo et al. 2000). The ever increasing spatial resolution of new instruments observing the solar corona will hopefully allow even more detailed studies of this kind.

A. Filter Ratio Diagnostic with TRACE data

Since it observes in different spectral bands, TRACE allows, in principle, to apply a filter-ratio diagnostic technique to obtain the temperature and the emission measure of the emitting plasma. For example, the fluxes ratio 195Å/171Å can be used to deduce plasma temperature and emission measure. On the other hand, because of the narrow band response, $R \equiv F_{195}/F_{171}$ is a multi-valued function of the temperature of the emitting plasma as clear from the upper panel of Fig. 12.

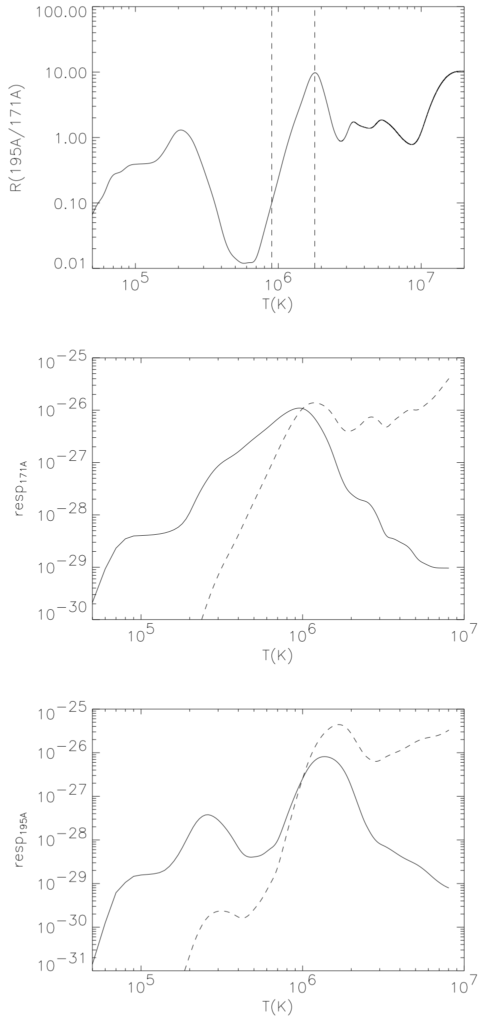

Fig. 12.— Upper panel – Filter ratio (195Å/171Å) vs. temperature; the dashed lines delimit the range considered by the *standard analysis* for the temperature derivation. Central and lower panel – The solid lines are the TRACE response curves in the two bands, 171Å (central panel) and 195Å (lower panel) (TRACE Analysis Guide; Bentley 2000); they are both in units of $\frac{DN}{sec\cdot(EM/A_{pixel})}$, where A_{pixel} is the area on the solar disk subtended by a pixel (i.e. $\sim 10^{15} cm^2$). The dashed lines show the TRACE sensitivity in these two narrow bands to the emission of plasma in hydrostatic loops with fixed semi-length, according to the model of Rosner, Tucker & Vaiana (1978).

In order to derive the temperature, the *standard analysis* of TRACE data forces the temperature to be in the range $0.9 \div 1.8 \cdot 10^6$ K where R(T) is invertible (range delimited by the dashed lines in upper panel of Fig. 12) and excludes any other temperature range. This choice is motivated by the temperature response of TRACE (see solid lines in central and lower panels of Fig. 12): indeed, 171Å and 195Å filter responses peak inside this range that nevertheless excludes temperature regions of high sensitivity in the two passbands. However this argument does not take into account the influence of the emission measure on the plasma visibility with TRACE and tends to give an isothermal view of loops that is probably inadequate and does not reflect the more complex density and temperature distribution of coronal loops that TRACE is able to observe. For example, if we consider the physics of coronal plasma confined in loops assuming Rosner, Tucker & Vaiana (1978) or Serio et al. (1981) hydrostatic model, we find that, for loops with fixed semi-length, approximately $n \propto T^2$ and then $EM \propto n^2 \propto T^4$, so the visibility with TRACE of the coronal confined plasma keeps high in the whole range $10^6 \div 10^7$ K as shown in Fig. 12.

In the light of the above considerations, we have developed a different analysis method (discussed in detail in section 3), that considers the plasma thermal structuring along the loop, to overcome the non-uniqueness in temperature and density derivation through filter ratio diagnostics for TRACE data.

This work has been partially supported with funds from "Progetti di Ricerca di Interesse Nazionale - MIUR" and from ASI. We acknowledge useful discussion and criticisms with L. Golub, E. DeLuca, H. Warren and their junior collaborators at CfA. We also acknowledge useful suggestions from an anonymous referee.

REFERENCES

Avni, Y. 1976, ApJ, 210, 642

Aschwanden, M.J., Nightingale, R.W., & Alexander, D. 2000, ApJ, 541, 1059

Bentley, R.D. 2000, SolarSoft TRACE Analysis Guide, Mullard Space Science Laboratory University College London

Brekke, P., Hassler, D., & Wilhelm, K., 1997, Sol. Phys., 175, 349

Colangelo, G., Pace, O., Marsden, R., & Fleck, B. 2000, ESA-bulletin 104

Dere, K.P., Landi, E., Mason, H.E., Monsignori Fossi, B.C., & Young, P.R. 1997, A&AS, 125, 149

Foukal, P. 1976, ApJ, 210, 575

Golub, L., Nystrom, G., Herant, M., Kalata, K., & Lovas, I. 1990, Nature, 344, 842

Gomez, D.O., Martens, P.C.H., & Golub, L. 1993, ApJ, 405, 767

Handy, B.N. et al. 1999, Sol. Phys., 187, 229

Lenz, D.D., DeLuca, E.E., Golub, L., Rosner, R., & Bookbinder, J.A. 1999, ApJ, 517, L155

Peres, G., & Orlando, S. 1996, ASP Conf. Ser., 9, 93

Priest, E.R., Foley, C.R., Heyvaerts, J., Arber, T.D., Culhane, J.L., & Acton, L.W. 2000, ApJ, 539, 1002

Reale, F., & Peres, G. 2000, ApJ, 528, L45

Rosner, R., Tucker, W.H., & Vaiana, G.S. 1978, ApJ, 220, 643

Schmelz, J.T., Scopes, R.T., Cirtain, J.W., Winter, H.D., & Allen, J.D. 2001, ApJ, 556, 896

Serio, S., Peres, G., Vaiana, G.S., Golub, L., & Rosner, R. 1981, ApJ, 243, 288

Tsuneta, S. et al. 1991, Sol. Phys., 136, 37

Vaiana, G.S., Krieger, A.S., & Timothy, A.F. 1973, Sol. Phys., 32, 81

Vaiana, G.S., & Rosner, R. 1977, ApJ, 216, 141

Vesecky, J., Antiochos, S., & Underwood, J. 1973, ApJ, 233, 987